

1 **Statistical characteristics of raindrop size**
2 **distribution during rainy seasons in Complicated**
3 **Mountain Terrain**

4 Wenqian Mao^{1,2,3,4}, Wenyu Zhang^{1,2,3,4*}, Menggang Kou¹Kou²

5 1. College of Resources and Environmental Sciences, Gansu Agricultural University, Lanzhou
6 730070, China

7 1-2. School of Geoscience and Technology, Zhengzhou University, Zhengzhou, 450001, China

8 2-3. Key Laboratory for Cloud Physics, Chinese Academy of Meteorological Sciences, Beijing
9 100081, China

10 3-4. College of Atmospheric Sciences, Lanzhou University, Lanzhou, 730000, China

11 Correspondence to: Wenyu-Wenqian MaoZhang (zhangwymdycmwq@zsu163.com.edu.cn)

12 **Abstract:** ~~+~~In order to improve understanding of the characteristics differences of
13 raindrop size distribution (DSD) ~~in~~over complex mountainous terrain, the
14 differences characteristics of in DSD ~~were analyzed by using the six months observation~~
15 ~~data at~~ over the southern slopes, northern slopes and interior of the inside in Qilian
16 Mountains were analyzed using six months of observations. For all rainfall events, the
17 number concentrations of small and large raindrops ~~on in~~ the interior inside and on the
18 southern slopes are were greater than ~~that~~ on the northern slopes, but midsize raindrops
19 ~~are were~~ less. The DSD spectrum of the interior was inside mountains are more variable
20 and differed significantly ~~differ~~ from that of the northern slopes. The differences in the
21 normalized intercept parameters of the DSD for stratiform and convective rainfall ~~are~~
22 were 8.3% and 10.4%, respectively, and those of the mass-weighted diameters ~~are were~~
23 10.0% and 23.4%, respectively, ~~while which~~ the standard deviations of DSD parameters
24 at interior on inside sites ~~are were~~ larger. The differences in the coefficient and exponent
25 of the Z-R relationship ~~are were~~ 2.5% and 10.7%, respectively, with an increasing value
26 of the coefficient from the southern slope to the northern slopes ~~in for~~ stratiform rainfall,
27 but the opposite ~~to for~~ convective rainfall. In addition, the DSD characteristics and Z-
28 R relationships ~~are were~~ more similar at the ipsilateral sites and ~~have had~~ smaller
29 differences between the southern slopes and interior of the inside mountains.

30
31 **Keywords:** ~~Raindrop~~raindrop size distribution; ~~Complicated~~complicated mountain
32 terrain; ~~spatial variation~~characteristic difference

带格式的: 字体: 倾斜

带格式的: 字体: 倾斜

34 **1 Introduction**

35 Raindrop size distribution (DSD), the number of raindrops per drop size per unit
36 volume, is an important parameter to statistically describe the microstructure of
37 precipitation (Bringi et al., 2003; Ma et al., 2019a). The measurement of DSD can
38 provide some fundamental information such as raindrop size (D), liquid water content
39 (W), rain rate (R), radar reflectivity factor (Z) and so on, which has an essential
40 contribution to improving quantitative precipitation estimates estimation (QPE) using
41 weather radar and satellite observations (Adirosi et al., 2018; Jash et al., 2019). The
42 parameterization of DSD can obtain the distribution model parameters of DSD in
43 different rain types, which is significant in advancing to advance microphysics
44 parameterization in numerical weather prediction (NWP) models (Wainwright et al.,
45 2014; McFarquhar et al., 2015; Zhao et al., 2019). In addition, understanding the DSD
46 is crucial in many applied application fields concerning hydrology, agriculture, soil
47 erosion and microwave communication (Rincon et al., 2002; Smith et al., 2009;
48 Angulo-Martínez et al., 2015; Lim et al., 2015; Yang et al., 2016).

49 Numerous studies have been carried out on the statistical characteristics of DSD
50 in different regions (Campos et al., 2006; Seela et al., 2017; Dolan et al., 2018; Protat
51 et al., 2019; Loh et al., 2019; Jash et al., 2019). It is has been shown that the number
52 concentration and size of raindrops increase with rain rate and so the DSD becomes
53 higher and wider. The characteristics in different rain types demonstrated display that the
54 mass-weighted mean diameter (i.e., D_m) and normalized intercept parameter (i.e., N_w)
55 of convective rainfall (CR) are larger than those of stratiform rainfall (SR).
56 Furthermore, these studies also reveal that there are more differences in the
57 characteristics of DSD. Dolan et al. (2018) divided global DSD characteristics into 6
58 types by using 12 datasets across three latitudes and found that the centralized regions
59 and DSD parameters of the 6 types varied in location. The average number of raindrops
60 in central Korea were was usually greater more numerous than that in the southeast
61 under three rainfall systems, especially drops on in the 0.31–0.81mm diameter range
62 (Loh et al., 2019). According to the DSD measurements in results from the Tibetan
63 Plateau (TP) region, it showed the eastern areas have are regions had higher raindrop
64 number concentration in the diameter range of of raindrops on 0.437–1.625 mm
65 diameters and more greater variation in on different diameters than that in central
66 areas regions (Wang et al., 2020). Compared to eastern China and northern China, the
67 DSD in southern China demonstrated shows a higher number concentration of
68 relatively small-sized drops, respectively (Zhang et al., 2019). The eComparison of the
69 Z-R relationship (defined as $Z=AR^b$) indicated indicates that the coefficient decreased
70 decreases with increasing R in the southern Tibetan Plateau TP, which is opposite in to
71 the case in sSouth China (Wu et al., 2017). For the DSD parameters of stratiform SR
72 and convective rainfall CR, there are various changes between the lower reaches and
73 middle reaches of the Yangtze River (Fu et al., 2020).

74 As reported in the above studies, DSD characteristics significantly vary
75 significantly with factors such as geographical location, climatic region and rain types.
76 Pu et al. (2020) analyzed the DSD characteristics of five sites in Nanjing city and found
77 the N_w of DSD to be was largest at site near industrial areas, but the D_m of DSD was

带格式的: 字体: 倾斜

带格式的: 字体: 倾斜

带格式的: 字体: 倾斜

78 largest at sites near ~~the~~ city's ~~cent~~center. In other words, even at ~~the~~ urban scale, there
79 are still differences ~~to in the~~ microphysical characteristics reflected by the DSD, which
80 is due to the influence of the surrounding environment. ~~How, Then, how~~ do the
81 characteristics of DSD vary from location ~~to location for over~~ the complicated mountain
82 terrain? Rao et al. (2006), ~~suggested that the obvious variation in DSD with altitude~~
83 ~~were related to evaporation and breakup~~ by comparing the DSD parameters at different
84 altitudes, ~~suggested that the obvious variation in DSD with altitude is related to the~~
85 ~~processes of evaporation and breakup. Using aircraft observations,~~ Geoffroy et al.
86 (2014) concluded that the total concentration of raindrops decreased while the average
87 drop size increased ~~as with~~ decreasing altitude, ~~which used aircraft observations. Then~~
88 ~~But~~ how large ~~would might be~~ the differences in DSD ~~be~~ at different altitudes in
89 mountainous regions? And ~~then~~ how significant ~~would might be~~ the effects ~~be~~ of these
90 differences?

91 ~~The~~ Qilian ~~mountains~~Mountains, a series of marginal mountains in the
92 northeastern part of ~~the Tibetan Plateau~~TP, are ~~the a~~ vitally important ecological
93 protection barrier in ~~the~~ northwest arid areas ~~of the region, which that~~ block the
94 connection ~~between~~of deserts and wilderness ~~in the northwest (shown as~~ Figure 1a).
95 The mountains form several inland rivers that are important water sources ~~s~~ for the
96 ~~northwest~~ arid areas ~~of the northwest~~ and have ~~therefore~~ made a considerable
97 contribution to regional economic development (Gou et al., 2005; Tian et al., 2014; Qin
98 et al., 2016). In this ~~paper~~study, we ~~choose~~ ~~the~~ Qilian ~~mountains~~Mountains as the
99 research object and selected ~~6 six~~ sites with different backgrounds representing the
100 southern slopes, northern slopes and ~~inside interior of~~ Qilian ~~the~~ mountains. To
101 thoroughly investigate the discrepancies in ~~the this complex~~complicated mountain
102 terrain, the DSD characteristics and Z-R relationships ~~are were~~ comprehensively
103 analyzed according to different rain types based on continuous disdrometer
104 observations in ~~the~~ rainy season. The primary goal ~~is was~~ to obtain ~~a deeper~~
105 ~~understanding and characteristic differences of DSD over~~ the ~~finer precipitation of~~
106 Qilian ~~mountains~~Mountains and improve the accuracy of QPE, which ~~would could~~
107 ~~then~~ be ~~used as a~~ research foundation for developing cloud water resources in
108 mountainous areas.

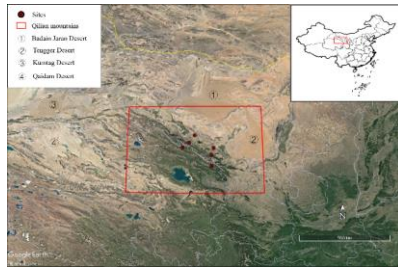
109 2 Data and method

110 2.1 Sites and instruments

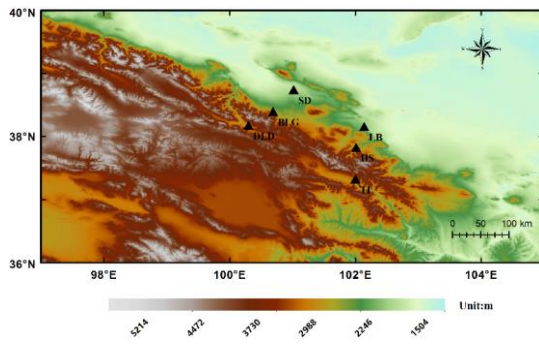
111 The eastern and middle sections of the Qilian Mountains were chosen as the main
112 study area, taking into account that several important inland rivers ~~originating originate~~
113 from these areas ~~of Qilian Mountains~~ (Li et al., 2019). Six disdrometers were deployed
114 on the southern slopes, northern slopes and ~~interior~~inside (close to the ridge) of ~~the~~
115 Qilian ~~mountains~~Mountains, with three sites in the eastern section ~~which~~ [called Taola
116 (TL), Huangchengshuiguan (HS), and Liuba (LB), from south to north], and ~~with~~
117 another three sites in the middle section ~~which~~ [called Daladong (DLD), Boligou (BLG),
118 ~~and~~ Shandan (SD), from south to north]. The background of ~~the~~ Qilian Mountains is
119 shown on the satellite map ~~in~~ Figure 1a, and the six sites are marked on the
120 topographical map, ~~also as in~~ Figure 1b. The distances between ~~the~~ six sites are listed in

带格式的: 字体: 倾斜

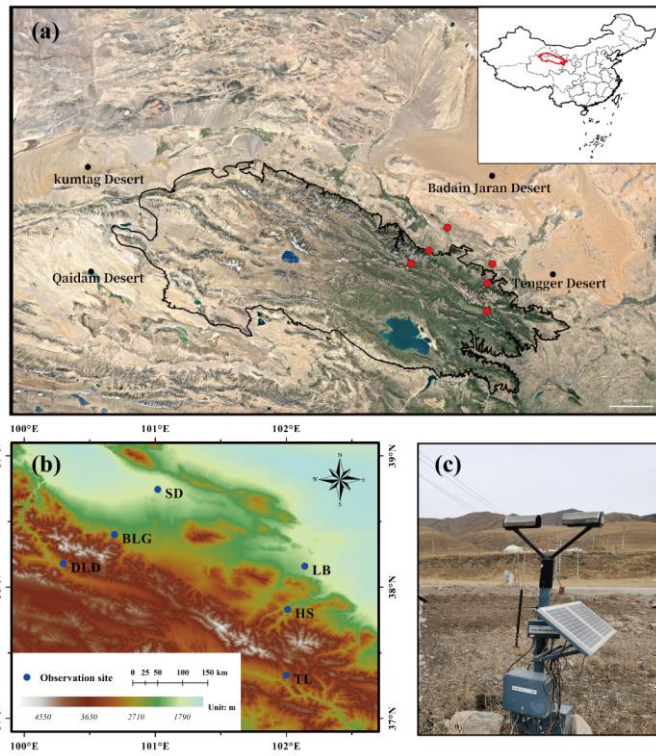
121 Table 1. The sites ~~on-in~~ the south, north and ~~interiorinside~~ are basically parallel to the
 122 ~~orientationtrend~~ of the mountains, and the sections formed by the sites in the east and
 123 ~~interiormiddle~~ are basically perpendicular to ~~the trend of the mountainit~~. ~~Through-On~~
 124 the ~~basis of an~~ historical weather review and rain gauge observations ~~results~~, the rainy
 125 season at the six sites is concentrated in May to October, with more precipitation in July,
 126 August and September.



127



128



129

130 Figure 1. The (a) Geographical overview of the Qian mountains Mountains; and (b) the
 131 disdrometer sites; the (circles) or triangles represent the location of the sites (c) the
 132 observation device at TL site. Source: The map above is from Google Earth © Google
 133 Earth YEAR

134 Table 1. Site details Location between every two sites (latitude, longitude, sea level
 135 height) and distances (km) between pairs of sites and distance information).

Six sites distance (km)	LB	HS	TL	SD	BLG	DLD
LB (38.16°N, 102.14°E, 1926m)	-	39.6	94.3	116.0	129.6	161.1
HS (37.83°N, 102.01°E, 2342m)	-	-	55.6	135.1	132.8	154.9
TL (37.33°N, 102.00°E, 2910m)	-	-	-	182.4	167.3	177.0
SD (38.80°N, 101.08°E, 1765m)	-	-	-	-	54.2	96.8
BLG (38.4°N, 100.69°E, 2455m)	-	-	-	-	-	43.3
DLD (38.18°N, 100.3°E, 2957m)	-	-	-	-	-	-

136 This experiment study used an optical, laser-based device to measure the DSD,
 137 called a DSG4 disdrometer (Figure 1c), which meets the assessment of Functional
 138 Specification Requirements For for Disdrometer issued by the China Meteorological
 139 Administration. The This disdrometer has the an HSC-OTT Parsivel2 sensor as the

140 observation part, manufactured by OTT Messtechnik (Germany) and Huatron (China).
 141 When raindrops pass through the horizontal flat laser beam generated by the
 142 transmitting part of the instrument, it causes ~~the~~ signal attenuation in the laser
 143 observation area. The raindrop size is determined by the degree of signal attenuation
 144 and the falling speed is recorded by the transit time. The sampling time is 60s and the
 145 velocity and drop sizes are divided into 32 non-equally spaced bins, varying from 0.05
 146 to 20.8 m s⁻¹ for velocity and 0.062 to 24.5 mm for drop diameter.

带格式的: 上标

147 2.2 Quality control of the data

148 It ~~is was~~ necessary to ~~carry out quality quality~~ control ~~on~~ the data ~~due to because of~~
 149 potential instrument error. Every minute of DSD ~~data has been carefully processed,~~
 150 ~~which~~ collected by the six DSG4 disdrometers from May to October 2020 ~~was carefully~~
 151 ~~processed. Specifically, the~~The following criteria ~~have been were~~ employed in choosing
 152 data for analysis. ~~(Jaffrain et al., 2011; Guyot et al., 2019; Pu et al., 2020):~~ (1) ~~The the~~
 153 first two size bins were ignored because of low signal-to-noise ratio; (2) samples with
 154 1-min total ~~of raindrop number of raindrops~~ less than 10, or ~~a~~ rain rate at ~~the~~ moment
 155 of discontinuous observation less than 0.1 mmh⁻¹ were regarded as noise; (3) raindrops
 156 ~~at the with~~ diameters ~~of~~ more than 8 mm were eliminated; (4) raindrops ~~s~~ with a falling
 157 terminal velocity $V(D_i)$ that ~~deviates deviated~~ from the empirical terminal velocity
 158 $V_{emp}(D_i)$ ~~by~~ more than 40% were removed (Kruger and Krajewski, 2002); and (5)
 159 samples with less than ~~5 five~~ bins after the correction of falling terminal velocity were
 160 deleted because ~~its their~~ DSDs ~~can't could not~~ be determined with too few bins. ~~The~~
 161 ~~fourth criterion can be expressed by the formula:~~

带格式的: 字体: 倾斜

带格式的: 字体: 倾斜

带格式的: 字体: 倾斜, 下标

带格式的: 字体: 倾斜

$$162 |V(D_i) - V_{emp}(D_i)| < 0.4V_{emp}(D_i) \quad (1)$$

163 where $V_{emp}(D_i) = 9.65 - 10.3\exp(-0.6D_i)$ (D_i is the mean volume-equivalent
 164 diameter of the i th size category), as derived from the formula given in Atlas et al.
 165 (1973).

带格式的: 字体: 倾斜

带格式的: 字体: 倾斜

166 After data quality control, the sample statistics of key steps are shown in Table 2.
 167 The number of 1-min DSD spectra selected from the six sites (LB, HS, TL, SD, BLG,
 168 DLD) after data quality control covering the rainy season (May–October) in the Qilian
 169 Mountains region in 2020 were 11103, 17619, 14814, 10736, 18861 and 13230,
 170 respectively, which accounted for 87.9%, 85.8%, 84.5%, 91.2%, 80.6% and 86.5% of
 171 the total number of samples.

172 Table 2. Sample statistics of data quality control at six sites

Samples	LB	HS	TL	SD	BLG	DLD
Total minutes (min)	12625	20536	17526	11770	23401	15289
Total minutes without noise (min)	12602	20509	17494	11756	23371	15267
After quality control (min)	11103	17619	14814	10736	18861	13230
Available rain minutes (%)	87.9%	85.8%	84.5%	91.2%	80.6%	86.5%

173

174 2.3 Integral parameters of rainfall

175 The basic observations obtained by ~~the~~ disdrometer ~~were theis~~ counts of raindrops

176 at each diameter and velocity. ~~Also, And~~ the diameters given by ~~the~~ disdrometers
 177 ~~were~~are the mid value of two adjacent bins, which we take ~~the diameters~~ as the
 178 corresponding endpoint bin values. The velocities ~~are~~ were the weighted average
 179 velocity class over the corresponding disdrometer. The raindrop number concentration
 180 $N(D_i)$ ($m^{-3} mm^{-1}$) in the i th size bin per unit volume per unit size interval for diameter
 181 ~~is~~ was calculated ~~by~~ the following equation:

$$182 \quad N(D_i) = \sum_{j=1}^{32} \frac{n_{i,j}}{A \cdot \Delta t \cdot V_j \cdot \Delta D_i} \quad (2)$$

183 ~~Where where~~ $n_{i,j}$ ~~denotes~~ is the counts of raindrops measured by ~~the~~ disdrometer within
 184 ~~the~~ size bin i and velocity bin j during ~~the~~ sampling time Δt ; A and Δt are the sampling
 185 area ($0.0054 m^2$) and sampling time ($60 s$), respectively; V_j ($m s^{-1}$) is the mid-value
 186 falling speed for velocity bin j ; ~~and~~ ΔD_i is the diameter spread for the i th diameter bin.

187 Some integral rainfall parameters, such as ~~the~~ total number concentration N_t
 188 (m^{-3}), rain rate R ($mm h^{-1}$), radar reflectivity factor Z ($mm^6 m^{-3}$) and liquid
 189 water content W ($g cm^{-3}$), can be derived by the following equations:

$$190 \quad N_t = \sum_{i=1}^{32} N(D_i) \Delta D \quad (3)$$

$$191 \quad R = \frac{6\pi}{10^4 \rho_w} \sum_{i=1}^{32} V(D_i) D_i^3 N(D_i) \Delta D_i \quad (4)$$

$$192 \quad Z = \sum_{i=1}^{32} N(D_i) D_i^6 \Delta D_i \quad (5)$$

$$193 \quad W = \frac{\pi \rho_w}{6 \times 10^3} \sum_{i=1}^{32} D_i^3 N(D_i) \Delta D_i \quad (6)$$

194 where ρ_w is ~~the~~ water density ($1.0 g cm^{-3}$); ~~and~~ $V(D_i)$ is the falling speed ~~measurements~~
 195 from ~~the~~ disdrometer. In this study, when calculating ~~the~~ rain rate we use $V_{emp}(D_i)$ to
 196 replace $V(D_i)$ because of measurement error, particularly at larger bins and faster falling
 197 speeds.

198 The ~~DSD~~ characteristics ~~of DSD~~ can be described by ~~a~~ three-parameter gamma
 199 distribution in ~~following the form introduced by Ulbrich (1983)~~. ~~Also, it has better~~
 200 ~~fitting capability than the M-P distribution on the broader variation of DSD fluctuations,~~
 201 ~~including the middle rain drops, especially on small and large rain scales.~~ ~~And it has~~
 202 ~~better capability than M-P distribution to describe the broader variation of DSD~~
 203 ~~fluctuations, which has been proven to be well fitted the main part of spectra and reduce~~
 204 ~~the fitting error on small and large scale.~~ ~~The three-parameter gamma distribution can~~
 205 ~~be expressed by the following formula:~~

$$206 \quad N(D) = N_0 D^\mu \exp(-\Lambda D) \quad (7)$$

207 where $N(D)$ is the raindrop number concentration; D is the raindrop bins with unit mm;
 208 ~~and~~ N_0 , μ and Λ are ~~the~~ intercept, shape and slope parameter from ~~the~~ three parameters
 209 of ~~the~~ gamma model, which can be derived from gamma moments or ~~the least-~~

带格式的: 字体: 倾斜

带格式的: 字体: 倾斜

带格式的: 字体: 倾斜

带格式的: 字体: 倾斜

带格式的: 字体: 倾斜

带格式的: 字体: 倾斜

带格式的: 字体: 倾斜

带格式的: 字体: 倾斜

带格式的: 字体: 倾斜

带格式的: 字体: 倾斜

带格式的: 字体: 倾斜

带格式的: 字体: 倾斜

带格式的: 字体: 倾斜

带格式的: 字体: 倾斜

带格式的: 字体: 倾斜

带格式的: 字体: 倾斜

带格式的: 字体: 倾斜

带格式的: 字体: 倾斜

210 squares/least-square method, respectively. When $\mu=0$, it degenerates into the M-P DSD
211 model.

212 Although, the gamma distribution is commonly accepted, the normalized gamma
213 distribution has also been widely adopted with its independent parameters and clear
214 physical meaning as follows (Dolan et al., 2018; Ma et al., 2019). Although, three-
215 parameter gamma distribution is commonly accepted model, the normalized gamma
216 model has been widely adopted with its independent parameters and clear physical
217 meaning as follows:

$$218 \quad N(D) = \frac{3}{128} N_w \left[\frac{(4 + \mu)^{(4+\mu)}}{\Gamma(4 + \mu)} \right] \left(\frac{D}{D_m} \right)^\mu \exp \left(-\frac{(4 + \mu)D}{D_m} \right) \quad (8)$$

219 Where μ is the shape parameter, which is in dimensionless; D_m (mm) is the mass-
220 weighted mean diameter, and N_w ($\text{m}^{-3} \text{mm}^{-1}$) is the normalized intercept parameter
221 computed from D_m . The form is as follows:

$$222 \quad D_m = \frac{\sum_{i=1}^{32} N(D_i) D_i^4 \Delta D_i}{\sum_{i=1}^{32} N(D_i) D_i^3 \Delta D_i} \quad (9)$$

$$223 \quad N_w = \frac{4^4}{\pi \rho_w} \left(\frac{10^3 W}{D_m^4} \right) \quad (10)$$

224 3 DSD parameter characteristics

225 3.1 Characteristics of DSD

226 The number of 1 min DSD spectra from six sites have been selected after data
227 quality control covering the rainy season (May–October) in the Qilian Mountains region
228 in 2020, which are accounted for 87.9%, 85.8%, 84.5%, 91.2%, 80.6%, 86.5% of the
229 total number of samples to LB, HS, TL, SD, BLG, DLD, respectively. Figure 2a shows
230 the mean DSDs for the six districts/sites during the rainy season in the Qilian
231 mountains/Mountains. The maximum concentration of raindrops is/was around on 0.562
232 mm in diameter and the maximum number concentration values of sites were order as
233 follows: are BLG>TL>DLD>HS>SD>LB. As the increasing diameter increased, the
234 number concentration values decreased and the concentration values followed the
235 order: are LB>SD>DLD>TL>BLG>HS at around 2 mm in diameter. When the diameter
236 is/was larger than 4 mm, the concentration of TL, BLG and HS are/was relatively high.
237 In this study, the data were/it is roughly divided into small raindrops (less than 1 mm in
238 diameter), midsize raindrops (1–3 mm) and large raindrops (greater than 3 mm) to
239 easily describe the difference of/in DSDs (Ma et al., 2019b; Pu et al., 2020). To highlight
240 the DSD differences caused by the background environment, Figure 2b shows the mean
241 DSDs normalized with/by the N_w and D_m results for the sites. Compared with Figure 2a,
242 the raindrop characteristics of the raindrops are/were more consistent across sizes, while
243 the differences between the above/sites are/were more pronounced, especially in the
244 midsize/medium and large raindrops, which truly reflects-reflected the DSD differences
245 caused by the location variability. Combining the characteristics of the geographical
246 environment of the six sites, we can analyze some differences in DSD characteristics in

带格式的: 字体: 倾斜

带格式的: 字体: 倾斜

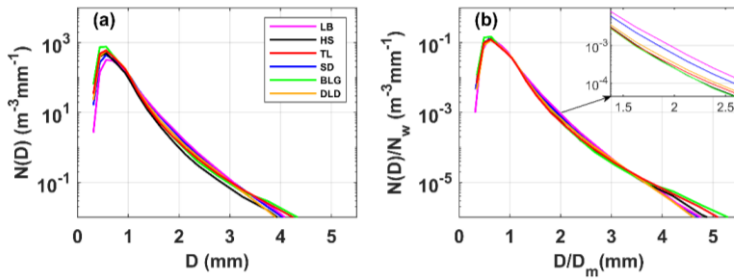
带格式的: 字体: 倾斜

带格式的: 字体: 倾斜

带格式的: 字体: 倾斜

带格式的: 字体: 倾斜

247 the Qilian Mountains. For small raindrops, the number concentrations ~~on the inside at~~
 248 ~~interior and southern-slopes sites were districts are~~ greater than ~~that on the at~~ northern-
 249 ~~slope sites~~; for midsize raindrops, the number concentrations ~~decrease-decreased~~
 250 sequentially ~~on-at~~ the northern-slopes, southern-slopes and ~~interior sites inside districts~~;
 251 ~~and~~ for large raindrops, the number concentrations ~~on-at~~ the ~~interior sites were inside~~
 252 ~~districts are~~ larger. In addition, the number concentrations of raindrops in the middle
 253 section of ~~this~~ the mountainous area ~~is-were~~ slightly greater than ~~that those~~ in the eastern
 254 section.



255 Figure-2. The (a) ~~Mean-mean measured DSDs; and~~ (b) ~~Normalized-normalized~~ mean
 256 ~~DSDs at six sites of in the~~ Qilian ~~mountains Mountains~~ region in ~~the~~ rainy season
 257

258 3.2 Distribution of DSD parameters

259 In order to study the differences in DSDs, we selected ~~6-six~~ integral rainfall
 260 parameters for discussion—~~namely, the, which are~~ normalized intercept parameter (N_w),
 261 mass-weighted mean diameter (D_m), shape parameter (μ), total number concentration
 262 (N_t), rain rate (R) and radar reflectivity factor (Z). Figure 3 and Table 2-3 show the
 263 distributions and statistics of ~~6-these six~~ DSD parameters (the distribution of each
 264 ~~parameter is was~~ normalized using the uniform method). ~~On average~~ ~~Averagely~~, D_m ~~is~~
 265 ~~was~~ more concentrated on smaller values at HS and BLG, which ~~shows showed~~ smaller
 266 mean values than TL and DLD, ~~while but~~ significantly more values greater than 1 mm
 267 at LB and SD; $\log_{10}N_w$ ~~is-was~~ more centralized on larger values at TL and DLD, with
 268 relatively smaller values at LB and SD; ~~and~~ the distribution patterns for μ and $\log_{10}N_t$
 269 ~~are-were~~ similar to those for $\log_{10}N_w$. The density curves of R and Z ~~are-were~~ similar,
 270 but there ~~are-were~~ differences ~~at among~~ the ~~6-six~~ sites, which ~~would be are~~ analyzed in
 271 detail ~~in subsequent content later in the paper~~. It is noteworthy that the frequency of
 272 samples with R around 0.6–1.0 mm h⁻¹ ~~is-was~~ highest, and samples with R less than
 273 1 mm h⁻¹ accounted ~~ed~~ for more than half of the total rainfall.

- 带格式的：字体：倾斜
- 带格式的：字体：倾斜
- 带格式的：字体：倾斜
- 带格式的：字体：倾斜
- 带格式的：字体：倾斜
- 带格式的：字体：倾斜
- 带格式的：字体：倾斜，下标
- 带格式的：下标
- 带格式的：字体：倾斜
- 带格式的：字体：倾斜，下标
- 带格式的：字体：倾斜
- 带格式的：下标
- 带格式的：字体：倾斜
- 带格式的：字体：倾斜，下标
- 带格式的：下标
- 带格式的：字体：倾斜
- 带格式的：字体：倾斜，下标
- 带格式的：字体：倾斜
- 带格式的：字体：倾斜
- 带格式的：字体：倾斜
- 带格式的：字体：倾斜

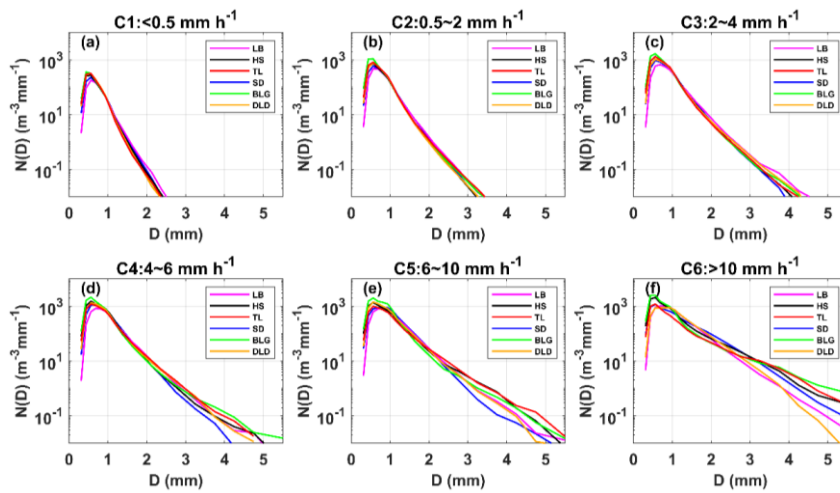
294 the number of samples and statistical values of the DSD parameters for the six classes.
 295 Clearly, Obviously, as the rainfall rate increased, with the rain rate class increasing,
 296 the number concentration of almost all raindrop sizes and the width of DSD shapes
 297 increased, and thus the tail of the DSD shape gradually moves/moved gradually towards
 298 a larger diameter, which are similar to the previous findings, studies such as those of Ma
 299 et al. (2019b) and Pu et al. (2020). Taking a number concentration of $0.01 \text{ m}^{-3}\text{mm}^{-1}$,
 300 the mean maximum diameter of DSD in each class was ordered as follows; is in order:
 301 2.3–2.5, 3.2–3.4, 3.9–4.5, 4.3–5.0, 5.0–5.6 and 6.0–7.0 mm (The the sixth-class
 302 diameter range is not fully shown in the figure). In class C1, the number concentrations
 303 are/were relatively similar in/at different sites; starting from class C2, the differences of
 304 in number concentration increased when the diameter is/was greater than 2 mm for 6
 305 the six sites; and the differences of in number concentration are/were gradually reflected
 306 on/in each raindrop size bin as the rainfall rate class increased/increasing.
 307 Observationally/Observingly, the DSDs of BLG, HS and TL have/had larger number
 308 concentrations in different rainfall rate classes, and the DSD parameters and standard
 309 deviations (SDs) are/were larger, especially for BLG.

310 Table 3-4. Statistics/Statistical of several integral DSD parameters for six rain rate
 311 classes at 6 six sites.

Class	Site s	Samples	$\log_{10}N_w$		D_m		μ		$\log_{10}N_t$		R		Z dB	Z dB
			$(\text{m}^{-3}\text{mm}^{-1})$		(mm)				(m^{-3})		(mm h^{-1})			
			ME	SD	ME	SD	ME	SD	ME	SD	ME	SD		
C1(<0.5 mm h ⁻¹)	LB	6520	3.25	0.41	0.88	0.18	12.36	7.09	1.74	0.34	0.20	0.13	12.6	4.40
	HS	10753	3.43	0.44	0.81	0.17	12.01	7.03	1.89	0.37	0.20	0.13	11.9	4.40
	TL	7858	3.52	0.44	0.79	0.16	12.91	7.12	1.96	0.37	0.20	0.13	11.7	4.40
	SD	5772	3.34	0.43	0.85	0.18	11.72	6.99	1.82	0.36	0.20	0.13	12.51	4.40
	BL	10073	3.50	0.48	0.79	0.17	12.94	7.28	1.94	0.40	0.20	0.13	11.73	4.26
	G													
C2(0.5~2 mm h ⁻¹)	DL	6891	3.51	0.43	0.79	0.15	13.04	6.92	1.96	0.36	0.21	0.13	12.14	4.15
	LB	3318	3.66	0.41	1.06	0.24	9.93	5.75	2.30	0.28	1.00	0.41	22.55	3.27
	HS	5700	3.82	0.39	0.97	0.21	10.21	5.88	2.44	0.26	0.96	0.37	21.67	3.09
	TL	5368	3.87	0.42	0.98	0.23	10.35	6.15	2.49	0.26	1.07	0.41	22.18	3.33
	SD	3778	3.73	0.41	1.03	0.23	9.94	6.14	2.36	0.28	1.02	0.40	22.40	3.15
	BL	6411	3.97	0.47	0.94	0.25	11.24	6.72	2.56	0.30	1.07	0.43	21.69	3.69
C3(2~4 mm h ⁻¹)	G													
	DL	4778	3.88	0.37	0.95	0.20	10.91	6.02	2.47	0.24	1.01	0.40	21.60	3.19
	LB	782	3.71	0.47	1.31	0.37	7.33	4.28	2.52	0.29	2.77	0.56	29.54	2.87
	HS	884	3.96	0.50	1.16	0.34	8.42	5.22	2.73	0.27	2.76	0.54	28.33	3.06
	TL	1232	4.00	0.47	1.13	0.33	8.70	5.93	2.75	0.23	2.68	0.53	28.07	3.16
	SD	812	3.89	0.44	1.19	0.27	8.57	5.53	2.63	0.26	2.71	0.53	28.41	2.68
BL	1865	4.05	0.49	1.11	0.30	8.62	5.75	2.81	0.25	2.70	0.53	27.99	3.29	
G														

C4(4~6 mm h ⁻¹)	DL	1111	3.91	0.44	1.18	0.29	7.81	5.45	2.70	0.23	2.74	0.54	28.73	3.09
	D													
	LB	229	3.80	0.47	1.41	0.40	7.33	3.94	2.65	0.31	4.76	0.57	32.69	2.63
	HS	191	4.03	0.54	1.28	0.47	7.54	4.42	2.86	0.27	4.80	0.56	31.70	3.34
	TL	213	3.84	0.56	1.41	0.51	6.23	4.64	2.77	0.28	4.77	0.54	32.82	3.54
	SD	187	4.03	0.41	1.24	0.27	8.35	5.02	2.80	0.22	4.76	0.54	31.32	2.52
	BL	321	3.99	0.66	1.33	0.53	7.97	6.10	2.93	0.27	4.78	0.54	32.44	4.40
G														
C5(6~10 mm h ⁻¹)	DL	270	3.92	0.53	1.35	0.47	6.50	4.80	2.83	0.25	4.83	0.56	32.55	3.47
	D													
	LB	167	3.81	0.46	1.55	0.44	6.46	3.38	2.72	0.27	7.66	1.22	35.74	2.85
	HS	49	3.69	0.74	1.70	0.68	6.89	4.82	2.75	0.38	7.42	1.09	36.14	4.29
	TL	103	3.57	0.62	1.78	0.66	5.20	4.62	2.71	0.32	7.32	1.02	37.03	3.76
	SD	128	3.96	0.39	1.42	0.35	7.10	3.96	2.82	0.21	7.68	1.17	34.76	2.42
	BL	138	3.97	0.76	1.51	0.80	8.34	6.35	2.99	0.27	7.37	1.02	35.09	4.96
G														
C6(>10 mm h ⁻¹)	DL	122	3.90	0.46	1.46	0.34	6.13	4.20	2.86	0.26	7.29	1.11	35.32	2.88
	D													
	LB	87	3.85	0.44	1.73	0.53	5.08	3.05	2.87	0.32	14.81	7.57	39.58	3.57
	HS	42	3.60	0.65	2.19	0.92	6.74	5.27	3.00	0.28	21.69	9.91	42.93	6.11
	TL	40	3.16	0.69	2.69	1.19	4.34	5.20	2.74	0.32	18.25	9.69	44.70	5.41
	SD	59	3.66	0.29	2.04	0.46	3.30	2.48	2.91	0.16	21.07	8.34	42.85	4.10
	BL	53	3.38	0.93	2.58	1.52	5.58	6.19	3.00	0.37	21.95	9.05	44.08	7.50
G														
	DL	58	3.82	0.47	1.80	0.46	6.64	4.12	2.84	0.28	16.58	7.21	40.13	3.53
	D													

312



313

314 Figure 4. Distribution of mean measured DSD for different rain rate classes at ~~6~~-six

315 sites.

316 Figure- 5 shows ~~box-and-whisker~~~~box-whisker~~ plots of the normalized intercept
317 parameter $\log_{10}N_w$ and mass-weighted mean diameter D_m for ~~6-six~~ sites ~~at-in~~ each rain
318 rate class. The middle line in the box indicates the median. The left and right lines ~~in~~
319 ~~the box~~ indicate the 25th and 75th ~~percentiles~~. The left and right ends of whiskers indicate
320 the most extreme data points between ~~the~~ 5th and 95th ~~percentiles~~, except outliers. The
321 median ~~of~~ D_m gradually ~~increases-increased~~ with a larger value range ~~when-as~~ the rain
322 rate class ~~increases-increased~~, particularly for HS and BLG ~~at-in~~ class C5 and C6. The
323 median ~~of~~ $\log_{10}N_w$ ~~increases-increased at-in~~ class C1 to C3 and then ~~tends-tended~~ to
324 decrease ~~at-in~~ class C5 to C6, ~~for~~ which the reduction ~~is-was~~ obvious at sites with a
325 larger value range, such as HS and BLG. Ma et al. (2019b) also ~~obtains-obtained~~ similar
326 conclusions about D_m and $\log_{10}N_w$. ~~The indication was~~~~It is indicated~~ that the increase ~~of~~
327 ~~in~~ rain rate ~~is-was~~ mainly due to the growth in raindrop size. ~~And-Also~~, the change ~~of~~
328 ~~in~~ number concentration may ~~be-have been~~ caused by the imbalance between the loss
329 of number concentration at small raindrop size and the addition at large raindrop sizes,
330 which ~~implies~~ in a sense ~~implies that thea~~ relationship ~~of-between the~~ collision-
331 coalescence and break-up of raindrops. It is worth noting that the microphysical
332 processes ~~are-were~~ quite different among the sites, ~~which-are-being~~ greatly influenced
333 by the surrounding environment. Because HS and BLG ~~are-were~~ located ~~on-in~~ the
334 ~~interior of theinside~~ mountains and close to ~~the~~ ridge, ~~thus~~ their dynamics and
335 thermodynamics as well underlying surfaces ~~are-were thus~~ different from ~~those of~~ other
336 ~~districts~~~~sites~~.

带格式的: 字体: 倾斜

带格式的: 字体: 倾斜

带格式的: 上标

带格式的: 上标

带格式的: 上标

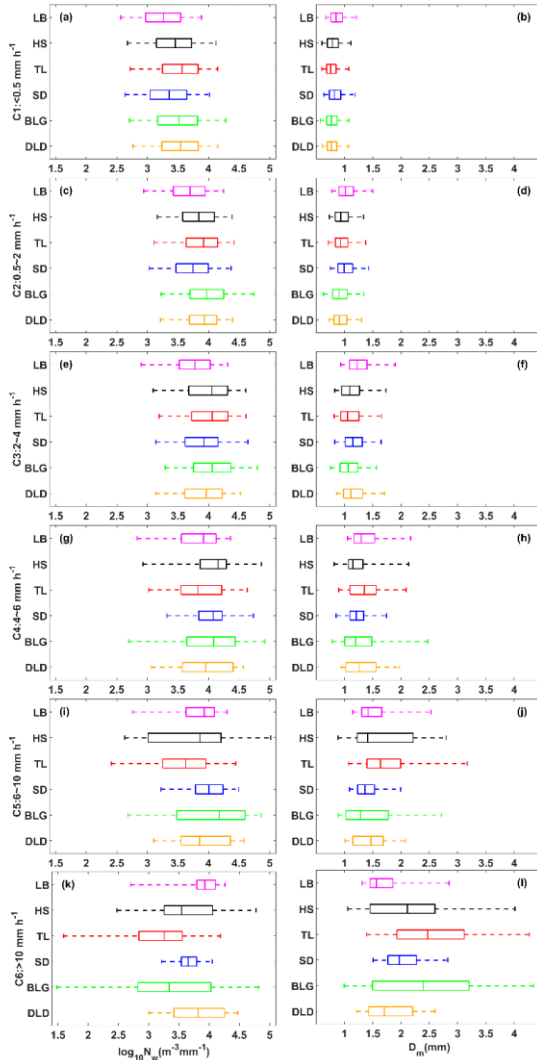
带格式的: 上标

带格式的: 字体: 倾斜

带格式的: 字体: 倾斜

带格式的: 字体: 倾斜

带格式的: 字体: 倾斜



337

338 Figure 5. Variation of the normalized intercept parameter $\log_{10}N_w$ (a) and the mass-
 339 weighted mean diameter D_m (b) for different rain rate classes at six sites. The three
 340 lines in the boxes are the 25th, 50th and 75th percentiles, from left to right, respectively.
 341 The whiskers on at the left end and right ends are the 5th and 95th percentiles,
 342 respectively. The colors represent the six sites same as in other figures.

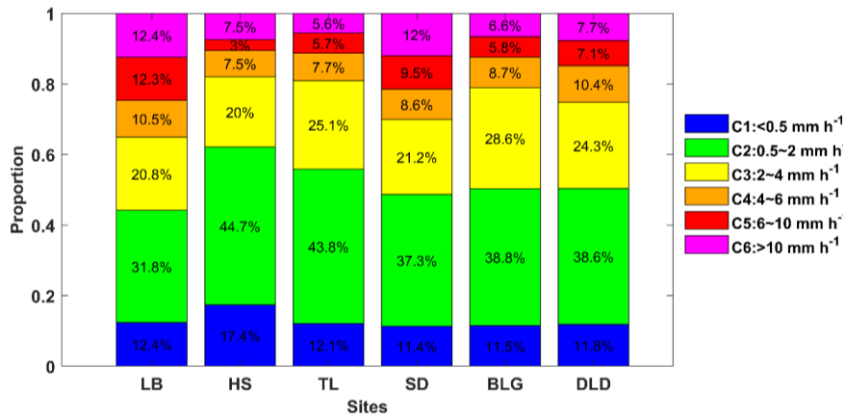
343

344 Figure 6 displays the contribution of different rain rate classes to the total rainfall
 345 at different sites. It is clear that C2 contributes contributed the most to the total rainfall
 346 of all sites, followed by C3, and the sum of the two classes of contribution could reach
 347 60% to of the total rainfall. Compared with the interior districts on the inside and
 southern slopes sites, C2 and C3 contributed slightly less to sites LB and SD sites

- 带格式的: 字体: 倾斜
- 带格式的: 字体: 倾斜
- 带格式的: 上标
- 带格式的: 上标
- 带格式的: 上标
- 带格式的: 上标
- 带格式的: 上标

348 (i.e., the northern slopes), while C5 and C6 contributed relatively more to sites LB and
 349 SD sites, indicating that there is a greater probability of heavy precipitation events on
 350 the northern slopes. The DSD parameters in Table 3 provide a more detailed
 351 representation of the rainfall differences between the three geographical
 352 sections/locations of the Qilian Mountains, i.e., namely the interior/inside, southern
 353 slopes and northern slopes. Meanwhile, it also reflects the characteristics of rainfall on
 354 in the eastern and interior/middle sections, such as the eastern section has had larger Z
 355 and D_m and smaller $\log_{10}N_w$ and $\log_{10}N_r$ compared to the interior/middle section. It is
 356 possible that there is a certain spatial connection between precipitation at the sites,
 357 which is related to the factors like such as the source of precipitation vapor, weather
 358 system and so on.

带格式的: 字体: 倾斜
 带格式的: 字体: 倾斜
 带格式的: 字体: 倾斜
 带格式的: 字体: 倾斜



359

360 Figure-6. Proportion of rainfall with different rain rate classes to rain amount at six
 361 sites.

362 3.4 DSD properties for different rain types

363 Previous studies on DSD have shown that there are significant differences in the
 364 DSD of convective and stratiform rainfall in the same climatic region, which has a
 365 substantial/great impact on the parameterization of NWP and remote sensing
 366 observations (Bringi et al., 2003; Penide et al., 2013). Due to the different physical
 367 mechanisms of convective and stratiform rainfall, it is possible/can be allowed to discuss
 368 the differences of/in microphysical structures for rainfall types through their DSD. In
 369 some studies, there have employed/used many different classification methods for
 370 rainfall types. Like example, Testud et al. (2001) used the rain rate; Chen et al. (2013)
 371 combined the rain rate and its standard deviation (SD); and the findings of Das et al.
 372 (2018) were based on the rain rate and radar reflectivity factor. Among these, the
 373 method from of Chen et al. (2013) has commonly been/was always used to establish
 374 samples of convective and stratiform rainfall, but mainly/in which the studies' area
 375 were concentrated in semi-humid or humid regions with relatively high rain rate and
 376 rainfall. However, the Qilian Mountains are located in the semi-arid regions of China
 377 and far from the sea, which/where the average rainfall rain and rainfall are quite

378 different from ~~the in~~ semi-humid regions. ~~The paper+T~~Therefore, ~~this paper~~ proposes a
379 new classification method for precipitation applicable to the arid and semi-arid regions
380 of ~~northwest~~Northwest China based on the classification ideas of Chen ~~et al. (2013)~~
381 and ~~Das et al. (2018)~~Saurabh.

382 Firstly, the sequences of DSD with continuous 1-min samples more than 10
383 minutes are determined, and R_t is defined ~~to denote as~~ the rain rate at time t . ~~The In the~~
384 first case~~-,~~ the R of samples from R_{t-5} to R_{t+5} are all less than 5 mm h^{-1} and their
385 ~~standard deviation (SD)~~ is less than 1.5 mm h^{-1} ; ~~in~~ the second case~~-,~~ the R of samples
386 from R_{t-5} to R_{t+5} are greater than or equal to 5 mm h^{-1} with more than ~~9-nine~~ samples
387 and their SD is greater than 1.5 mm h^{-1} ; ~~and in~~ the third case~~-,~~ ~~the situation is the same~~
388 as the second case but their SD is less 1.5 mm h^{-1} . Secondly, samples satisfying $Z < 20$
389 and $W < 0.08$ in the second case are removed (Thurai et al., 2016; Das et al., 2018). And
390 then, samples with R_t greater than or equal to 5 mm h^{-1} in the second case are regarded
391 as convective rainfall and samples with R_t less than 5 mm h^{-1} in the second case are
392 regarded as transition~~al~~ rainfall (the rainfall stage in which convective precipitation
393 develops and declines). Samples in the first case are regarded as stratiform rainfall.
394 Through experiments, the third case does not exist.

395 The $\log_{10}N_w$ and D_m of different rainfall types ~~are-were~~ different, which ~~were~~
396 ~~takenmake~~ as the main research objects. Figure 7 shows the variation of $\log_{10}N_w$ with
397 ~~the-~~ D_m at different sites. The blue, red, and yellow scattered points represent stratiform,
398 convective and transition~~al~~ rainfall, respectively. Obviously, there are fairly clear
399 boundaries between the scatter points for ~~the~~ different precipitation type events, and the
400 same dividing line can be used to distinguish ~~between the~~ different rainfall types at
401 different sites. The black solid lines were drawn based on visual examination of the data
402 with a slope of approximately -1.60 and intercept of 6.008 to represent the split
403 between stratiform, transition~~al~~ and convective rainfall in all subplots. The black dashed
404 line can distinguish transition~~al~~ rainfall (transition~~al~~ and stratiform rainfall have ~~an~~
405 overlap area) with a slope of approximately -3.338 and intercept of 6.847 . Note that
406 the dividing line between stratiform and convective rainfall has the same slope ~~as that~~
407 obtained by Bringi et al. (2003) (solid green line with a slope of -1.6 and intercept of
408 6.3), ~~who fitted the~~ composite results based on disdrometer data and from radar
409 retrievals covering many climate conditions from near ~~the~~ equator to plateau. The
410 $\log_{10}N_w$ and D_m from the figures ~~to-for~~ stratiform, convective and transition~~al~~ rainfall
411 are respectively concentrated in ~~the ranges of~~ $3.1-3.9 \text{ m}^{-3}\text{mm}^{-1}$, $0.75-1.1 \text{ mm}$; $3.8-$
412 $4.2 \text{ m}^{-3}\text{mm}^{-1}$, $1.4-1.6 \text{ mm}$; $3.6-4.0 \text{ m}^{-3}\text{mm}^{-1}$, $1.05-1.2 \text{ mm}$. Compared to the
413 maritime-like cluster and continental-like cluster of convective rainfall proposed by
414 Bringi et al. (2003), the convective events in ~~the~~ Qilian Mountains are more consistent
415 with the continental-like cluster (the gray rectangle with smaller $\log_{10}N_w$ and larger D_m
416 in ~~Figure-Fig.~~ 7). There are isolated convective events in the maritime-like cluster, but
417 it is difficult to have more events from the trend between $\log_{10}N_w$ and D_m . This is also
418 consistent with ~~the~~ features of ~~the~~ geographical location ~~in-of the~~ Qilian Mountains.

带格式的: 字体: 倾斜

带格式的: 字体: 倾斜, 下标

带格式的: 字体: 倾斜

带格式的: 字体: 倾斜

带格式的: 字体: 倾斜

带格式的: 字体: 倾斜

带格式的: 字体: 倾斜

带格式的: 字体: 倾斜

带格式的: 字体: 倾斜

带格式的: 字体: 倾斜

带格式的: 字体: 倾斜

带格式的: 字体: 倾斜

带格式的: 字体: 倾斜

带格式的: 字体: 倾斜

带格式的: 字体: 倾斜

带格式的: 字体: 倾斜

带格式的: 字体: 倾斜

带格式的: 字体: 倾斜

带格式的: 字体: 倾斜

带格式的: 字体: 倾斜

带格式的: 字体: 倾斜

带格式的: 字体: 倾斜

带格式的: 字体: 倾斜

带格式的: 字体: 倾斜

带格式的: 字体: 倾斜

带格式的: 字体: 倾斜

带格式的: 字体: 倾斜

带格式的: 字体: 倾斜

带格式的: 字体: 倾斜

带格式的: 字体: 倾斜

带格式的: 字体: 倾斜

带格式的: 字体: 倾斜

带格式的: 字体: 倾斜

带格式的: 字体: 倾斜

带格式的: 字体: 倾斜

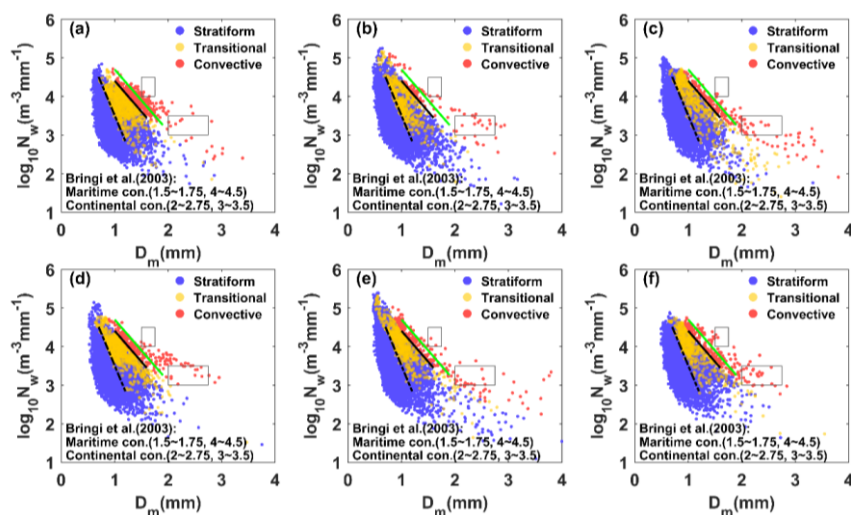
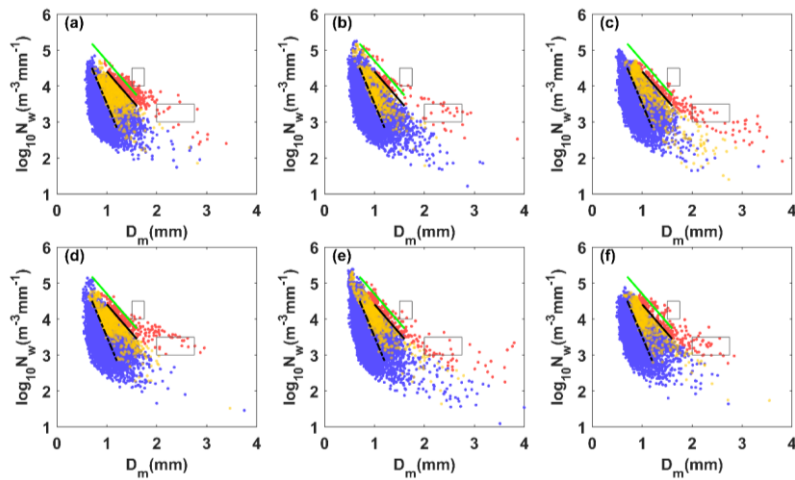
带格式的: 字体: 倾斜

带格式的: 字体: 倾斜

带格式的: 下标

带格式的: 字体: 倾斜

带格式的: 字体: 倾斜



419

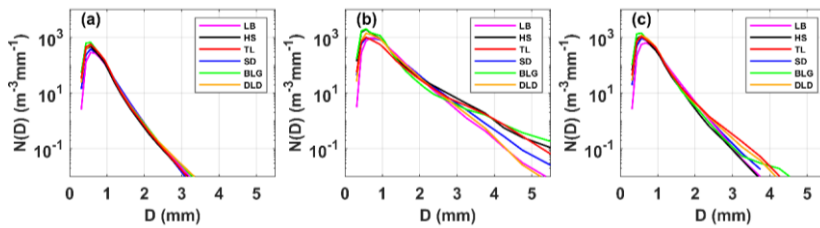
420

421 Figure 7. Scatter plot of $\log_{10}N_w$ versus D_m for different rain types at (a) LB, (b) HS,
 422 (c) TL, (d)SD, (e)BLG, and (f)DL. The stratiform cases, convective cases and
 423 transitional cases are represented by blue, red and yellow scatter points, circle dots,
 424 respectively. The black dashed lines are the $\log_{10}N_w-D_m$ relationship for stratiform
 425 versus convective cases and stratiform versus transitional case.

- 带格式的: 字体: 倾斜
- 带格式的: 字体: 倾斜
- 带格式的: 字体: 倾斜, 下标
- 带格式的: 字体: 倾斜
- 带格式的: 字体: 倾斜

426 Figure 8 shows the mean DSDs for stratiform, convective and transitional rainfall
 427 at the six sites. The range of number concentrations and corresponding raindrop
 428 diameters for the three types were significantly different, matching the basic
 429 characteristics of DSD. The mean DSDs of stratiform rainfall differed slightly among
 430 the sites; convective rainfall has had big differences at among the sites; and transitional
 431 rainfall presented appears more differences beginning at larger than 2.2 mm in diameter,

432 which ~~are~~ were the expected results. Stratiform rainfall usually has a large horizontal
 433 extent and ~~an~~ homogeneous cloud distribution, which makes the DSD characteristics
 434 basically ~~the~~ same under the influence of ~~the~~ same cloud system in ~~the~~ mountainous
 435 areas. ~~However,~~ But convective rainfall is related to ~~the~~ local thermal and dynamical
 436 factors, which could lead to differences in ~~the~~ DSD at different sites ~~adding~~ when
 437 ~~considering~~ the complex topography and diverse underlying ~~surfaces~~ in mountainous
 438 areas. For example, ~~in~~ for convective rainfall, there ~~is~~ was a significant increase in the
 439 number concentration of raindrops larger than 2.2 mm ~~in~~ diameter at BLG, HS and TL,
 440 indicating that these ~~districts~~ sites are conducive to the development of convective
 441 precipitation. ~~Also,~~ And the number concentration of small raindrops ~~in~~ at BLG and HS
 442 ~~is~~ were higher than ~~that~~ ~~in~~ at TL (the southern slope), which may be due to the higher
 443 altitude of the ~~interior~~ inside sites reducing the falling distance of raindrops after exiting
 444 the cloud and decreasing the impact of collision on the raindrop evolution. In other
 445 words, even ~~in~~ for the same rainfall type, the ~~microphysics~~ microphysical process of
 446 rainfall at different sites is still different, depending on the topography and position of
 447 the observation point relative to the cloud base.



448
 449 Figure 8. Distribution of mean measured DSD for (a) stratiform rainfall, (b) convective
 450 rainfall and (c) transitional rainfall at six sites.

451 Figure 9 ~~is~~ shows box-and-whisker plots of $\log_{10}N_w$ and D_m for different rain
 452 types. The $\log_{10}N_w$ and D_m of stratiform rainfall ~~are~~ were smaller than ~~that~~ those of
 453 convective rainfall but larger than ~~that~~ those of transitional rainfall. Sites with a large
 454 $\log_{10}N_w$ value range ~~have~~ had a larger values ranges for D_m ; and sites with a large
 455 median ~~for~~ $\log_{10}N_w$ ~~have~~ had a smaller median ~~for~~ D_m , especially at sites HS and BLG
 456 ~~for~~ sites in convective rainfall. Based on the mean values of ~~the~~ six sites in Table 45, the
 457 DSD characteristics in ~~the~~ Qilian Mountains consists of a larger N_w and ~~a~~ smaller D_m
 458 due to ~~the~~ melting of tiny, compact graupel, and rimed ice particles (relative to large,
 459 low-density snowflakes). Compared with transitional rainfall, the D_m of convective
 460 rainfall ~~is~~ was obviously larger, indicating that the increase in rain rate in this area is
 461 mainly due to the growth in raindrop size. Moreover, ~~on~~ the northern slopes ~~one~~ should
 462 consider the increase ~~of~~ in number concentration, because the $\log_{10}N_w$ of convective
 463 rainfall also ~~have~~ increased. Note that the number of convective samples on the northern
 464 slopes ~~is~~ was higher than that of other sites, which corresponds to the speculation ~~in~~
 465 ~~regarding~~ the contribution of different rain rate classes. On average, ~~of~~ for stratiform
 466 rainfall, the dispersion degree of $\log_{10}N_w$ and D_m ~~in~~ at different sites ~~is~~ was 8.3% and
 467 10.0%, respectively; and ~~for~~ convective rainfall ~~it~~ was 10.4% and 23.4%,
 468 respectively. The ~~SD~~ standard deviations of DSD parameters at sites HS and BLG sites

带格式的: 字体: 倾斜
 带格式的: 字体: 倾斜
 带格式的: 字体: 倾斜
 带格式的: 字体: 倾斜
 带格式的: 字体: 倾斜
 带格式的: 字体: 倾斜
 带格式的: 字体: 倾斜
 带格式的: 字体: 倾斜
 带格式的: 字体: 倾斜
 带格式的: 字体: 倾斜
 带格式的: 字体: 倾斜
 带格式的: 字体: 倾斜

带格式的: 字体: 倾斜
 带格式的: 字体: 倾斜

469 ~~are~~ were relatively large.

470 Table 4-5 ~~Statistics~~ Statistical of several integral DSD parameters for six sites with
 471 stratiform rainfall, convective rainfall and transitional rainfall

Type	Sites	No. samples	$\log_{10}N_w$		$D_{0.1}$		μ		$\log_{10}N_r$		R		Z
			(m ⁻³ mm ⁻¹)		(mm)				(m ⁻³)		(mm h ⁻¹)		dBZ
			ME	SD	ME	SD	ME	SD	ME	SD	ME	SD	ME
S	LB	7123	3.42	0.42	0.96	0.21	11.48	7.98	1.98	0.38	0.54	0.60	16.93
	HS	12694	3.60	0.44	0.88	0.21	11.24	7.89	2.14	0.40	0.54	0.58	16.17
	TL	10091	3.71	0.43	0.87	0.20	11.90	8.01	2.23	0.39	0.65	0.67	16.85
	SD	7175	3.51	0.44	0.95	0.22	11.15	8.03	2.07	0.39	0.62	0.64	17.36
	BLG	12467	3.72	0.49	0.88	0.23	12.24	8.50	2.25	0.44	0.70	0.74	17.11
	DLD	9685	3.70	0.42	0.88	0.21	11.91	7.91	2.23	0.38	0.67	0.69	17.18
C	LB	292	3.91	0.35	1.49	0.35	6.50	3.30	2.81	0.23	9.28	5.56	35.88
	HS	100	3.85	0.67	1.71	0.84	6.33	4.33	2.95	0.30	12.55	13.75	37.32
	TL	159	3.54	0.59	1.87	0.74	5.21	4.97	2.72	0.30	9.48	6.91	37.96
	SD	219	3.91	0.37	1.54	0.47	6.61	4.68	2.85	0.19	10.75	7.68	36.24
	BLG	198	3.91	0.74	1.64	0.97	8.00	7.37	3.00	0.27	10.57	15.49	36.29
	DLD	203	3.94	0.48	1.50	0.43	6.96	5.24	2.87	0.27	9.41	6.04	35.89
T	LB	787	3.76	0.39	1.15	0.21	8.37	4.35	2.47	0.31	2.16	1.25	26.42
	HS	541	3.89	0.49	1.05	0.29	8.98	6.74	2.59	0.33	1.81	1.15	24.79
	TL	465	3.77	0.70	1.22	0.49	8.81	6.91	2.56	0.44	2.30	1.21	27.10
	SD	819	3.87	0.41	1.12	0.26	8.23	5.46	2.59	0.28	2.28	1.18	26.59
	BLG	665	4.04	0.51	1.04	0.31	10.33	7.31	2.72	0.33	2.19	1.13	25.66
	DLD	503	3.95	0.46	1.10	0.30	8.69	6.16	2.67	0.31	2.35	1.17	26.60

带格式的: 字体: 倾斜

带格式的: 字体: 倾斜

带格式的: 字体: 倾斜, 下标

带格式的: 字体: 倾斜

带格式的: 字体: 倾斜

带格式的: 字体: 倾斜

带格式的: 字体: 倾斜

带格式的: 字体: 倾斜

带格式的: 字体: 倾斜

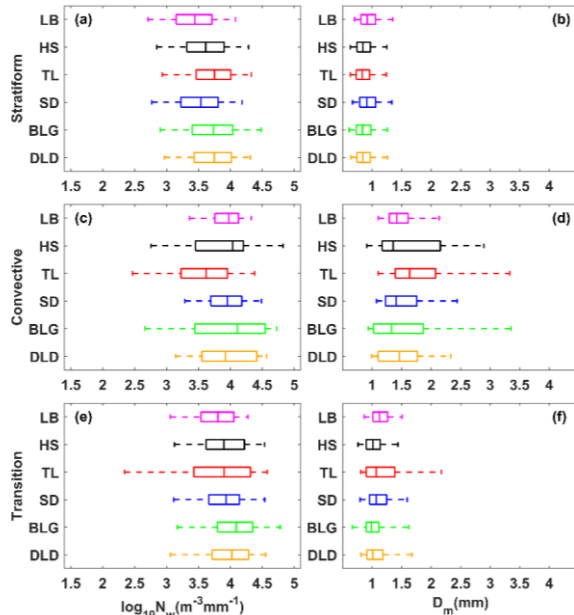


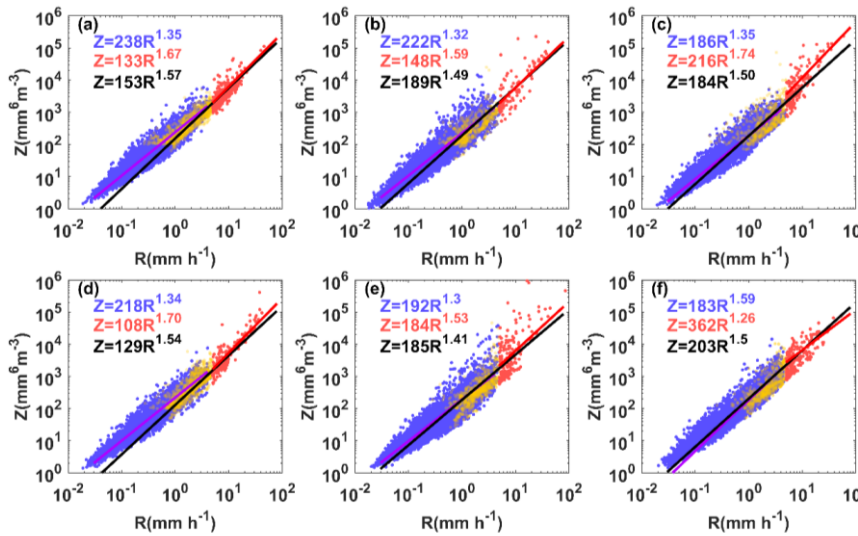
Figure 9. Same as As in Fig. 5 but for different rain types at six sites.

3.5 Implications for radar rainfall estimation with DSD

The sixth moment of raindrop diameter is proportional to the radar reflectivity factor and the 3.76th moment is approximately the rain rate (they can be calculated by Equations 4 and 5). Generally, the theoretical basis of the QPE for single polarization radar (ground-based or space-based) is the power relationship between the radar reflectivity and rainfall rate ($Z=AR^b$). This makes the coefficients A and exponents b of the power relationship heavily dependent on the variation of the DSD. Therefore, it is necessary to obtain the A and b of different sites according to different rainfall types.

Figure 10 shows the $Z-R$ scatter plots for different sites and the fitted power-law relationships for different rainfall types. The blue and red scatter points represent stratiform and convective rainfall, respectively. The purple, red and black solid lines indicate the $Z-R$ relationships for stratiform, convective and total rainfall, respectively. It shows that the $Z-R$ scatter points for HS and BLG are relatively scattered around the 5 mm h⁻¹ rain rate. Besides, the $Z-R$ relationship of total rainfall underestimates the stratiform rainfall at low R values and underestimates the convective rainfall at high R values. Based on the average of $Z-R$ relationship using a least-squares method, the dispersion degree of A and b at different sites was 42.5% and 10.7%, respectively, which reveals there to be large differences in mountain areas.

- 带格式的：字体：倾斜
- 带格式的：字体：倾斜
- 带格式的：字体：倾斜
- 带格式的：字体：倾斜
- 带格式的：字体：倾斜
- 带格式的：上标
- 带格式的：字体：倾斜
- 带格式的：字体：倾斜
- 带格式的：字体：倾斜
- 带格式的：字体：倾斜



492

493

494

495

496

497

Figure 10. Scatter plots of Z (mm^6m^{-3}) versus R (mm h^{-1}) for three rain types at (a) LB, (b) HS, (c) TL, (d)SD, (e)BLG, and (f)DLD. The blue, red and yellow scatter points represent stratiform, convective and transitional cases, respectively. The purple, red and black lines denote the Z - R relationships. The blue, red and black formula denote stratiform, convective and total Z - R relationships.

498

499

500

501

502

503

504

505

506

507

508

509

510

511

512

513

514

515

In order to compare the six sites Z - R relationships with some standard Z - R relationships, the results for $Z=300R^{1.4}$ for convective rainfall commonly used on-in radar, and $Z=200R^{1.6}$ (i.e., M48) for stratiform rainfall commonly used on-in midlatitude areas, are provided in Figure 11. Overall, convective rainfall has had smaller values of A and larger values of b than that those of stratiform rainfall (excluding DLD). The A values of convective rainfall are were smaller than the commonly used Z - R relationship with large differences, but the b values are were greater. The distribution of A and b for stratiform rainfall is was relatively concentrated, with A and b ranging from 186–238 and 1.3–1.35, respectively. The A values of SR are were close to the those of M48, and the b values are were close to and smaller than the Z - R of global SR. Station The DLD station has had a similar Z - R in-for stratiform rainfall with as M48, while its convective rainfall is was different from other sites, with a larger A value (twice as large as other sites) and smaller b value. In addition, it can make it is clear that the A value of stratiform rainfall increases-increased from the southern slopes to northern slopes, while the opposite was the case for convective rainfall is opposite. And Also, the Z - R relationships of the same sections side are more consistent, such as both on those of the interior inside or the northern slopes, which have distinct geographic characteristics.

带格式的: 字体: 倾斜

带格式的: 上标

带格式的: 字体: 倾斜

带格式的: 字体: 倾斜

带格式的: 字体: 倾斜

带格式的: 字体: 倾斜

带格式的: 字体: 倾斜

带格式的: 字体: 倾斜

带格式的: 字体: 倾斜

带格式的: 字体: 倾斜

带格式的: 字体: 倾斜

带格式的: 字体: 倾斜

带格式的: 字体: 倾斜

带格式的: 字体: 倾斜

带格式的: 字体: 倾斜

带格式的: 字体: 倾斜

带格式的: 字体: 倾斜

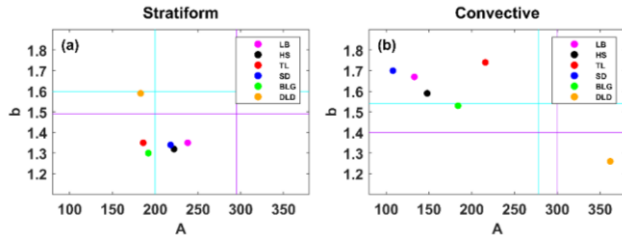
带格式的: 字体: 倾斜

带格式的: 字体: 倾斜

带格式的: 字体: 倾斜

带格式的: 字体: 倾斜

带格式的: 字体: 倾斜



516

517 Figure 11. The A and b values of the Z - R relationships for (a) stratiform rainfall and (b)
 518 convective rainfall at six sites. The purple lines in Fig. 12(a) and cyan lines in (b)
 519 correspond to the global Z - R model ($Z = 295R^{1.49}$ for continental stratiform rainfall and
 520 $Z = 278R^{1.54}$ for convective rainfall, respectively) (Ghada et al., 2018). The cyan lines
 521 in Fig. 12(a) represents the midlatitude stratiform rainfall Z - R model ($Z = 200R^{1.60}$,
 522 Marshall, 1948); and the cyan-purple lines in Fig. 12(b) represents the convective
 523 rainfall Z - R model ($Z = 300R^{1.40}$) applied to the operational weather radar (Fulton et al.,
 524 1998).

525 4 Discussion

526 The paper analyses the statistical characteristics of DSD at different sites in the
 527 Qilian Mountains during the rainy season, which not only contain rainfall classes and
 528 rainfall types but more importantly reflect the differences between different sites. The
 529 results from different aspects can be mutually confirmed and have a good representation
 530 of the spatial distribution, making serving as a strong great factual basis for the
 531 discussion of the microphysical structure for of precipitation. For example, with the rain
 532 rate class rising, the number concentration of all size bins is increased and the width of
 533 DSDs become became wider, which as a feature are manifested in rain types that as
 534 convective rainfall has having a larger rain rate. In spatial terms of spatiality, the
 535 characteristics of precipitation on in the interior of the mountains inside and on the
 536 southern slopes are were closer, whether considering the overall DSD distribution or the
 537 distributions of DSD parameters distribution. But However, there are some were
 538 obvious variabilities in at the interior sites inside mountains for DSD parameters due to
 539 the influences of its local dynamics and thermal effects. On the other hand, these
 540 characteristics also exhibited some differences between the interior middle and eastern
 541 sections of the in Qilian Mountains, especially in the discussion of DSD parameters for
 542 rainfall classes and rainfall types (shown as Figures 5 and 9). This spatial variation in
 543 DSD suggests that microphysical processes involved in the DSD are influenced by
 544 complex topography (altitude, mountain alignment) and potentially related to the source
 545 of water vapor, development of precipitation process and anthropogenic factors.

546 Compared to the precious previous studies that are focused on eastern, southern
 547 and northern China as well the Tibetan Plateau, the Qilian Mountains region have has
 548 its own unique DSD characteristics and Z - R relationship during the rainy season, which
 549 include including the a smaller raindrop diameter with a higher number concentration.
 550 Moreover, the division of rainfall rate classes in the Qilian Mountains more adequately
 551 reflects the DSD characteristics at in each class, unlike when using the classification

- 带格式的: 字体: 倾斜
- 带格式的: 字体: 倾斜
- 带格式的: 字体: 倾斜
- 带格式的: 字体: 倾斜
- 带格式的: 字体: 倾斜
- 带格式的: 字体: 倾斜
- 带格式的: 字体: 倾斜
- 带格式的: 字体: 倾斜
- 带格式的: 字体: 倾斜
- 带格式的: 字体: 倾斜

552 method of other sites with larger rainfall rates. More importantly, the proposed
553 classification of stratiform and convective rainfall can clearly distinguish between the
554 distribution of $\log_{10}N_w$ versus D_m in different rainfall types, for which the dividing line
555 (slope of -1.6 and intercept of 6.008) between stratiform and convective rainfall has
556 the same slope as the line (slope of -1.6 and intercept of 6.3) given by Bringi et al
557 (2003). Furthermore, according to this method, it can be easily proven that convective
558 events are more consistent with the continental-like cluster, conforming to the
559 precipitation characteristics of the Qilian Mountains. Above all, it is Qilian Mountains
560 that the proposed classification of stratiform and convective rainfall is applicable to,
561 which is located on the arid and semi-arid regions.

带格式的: 字体: 倾斜

带格式的: 字体: 倾斜

562 As aforementioned above, the characteristics of DSD mainly describe on the
563 diameters larger than 0.2 mm, which is are limited by the observation instruments being
564 unable to that cannot detect the small drops on of diameter less than 0.2 mm. So Therefor,
565 it is not a complete DSD, and underestimates the number concentration of small drops
566 on of diameter less than 0.5 mm is underestimated. Recent studies have been devoted
567 to improving DSD observations in order to overcome the limitations of disdrometers.
568 A study by Thurai et al. (2017) have obtained a more complete DSD by splicing the
569 2DVD and MPS (Meteorological Particle Spectrometer) measurements to observe
570 DSDs and developed a technology to reconstruct the drizzle-mode DSD (Raupach et
571 al., 2019), which has a good presentation to of the DSD of small raindrops was provided,
572 and more important applications were highlighted.

573 5 Summary and conclusion

574 Based on the six months of DSD data observed in over the southern slopes,
575 northern slopes and interior of the inside of Qilian Mountains, the characteristics and
576 their differences of DSD are were studied, and the Z-R relationships of six districts sites
577 are were discussed. The main conclusions can be summarized are as follows:-
578

带格式的: 字体: 倾斜

579 For small raindrops, the number concentrations on the inside and southern slopes
580 districts are greater than that on the northern slopes; for midsize raindrops, the number
581 concentrations decrease sequentially on the northern slopes, southern slopes and inside
582 districts; for large raindrops, the number concentrations on the inside districts are larger.
583 In addition, the number concentrations of raindrops in the middle section of the
584 mountainous area is slightly greater than that in the eastern section.

584 1. For all rainfall events, the number concentrations of small and large raindrops on
585 in the interior inside and on the southern slopes are were greater than that on the
586 northern slopes, while midsize raindrops are were less. The DSD of the interior of
587 the inside mountains showed has a great variability, mainly in terms of the $\log_{10}N_w$
588 and D_m (DSD parameters), which is was quite different to the case for from the
589 northern slopes.

带格式的: 字体: 倾斜

带格式的: 字体: 倾斜

590 2. The rainfall rates DSDs are were divided into six categories based on rainfall
591 rate the DSD characteristics: C1, $R < 0.5$; C2, $0.5 \leq R < 2$; C3, $2 \leq R < 4$; C4, $4 \leq R < 6$;
592 C5, $6 \leq R < 10$; and C6, $> 10 \text{ mm h}^{-1}$. As the rainfall rate increases increased, the
593 median of D_m for each station is gradually larger and the median of N_w rises on
594 C1-C3 and then decreases on C4-C6, as well the differences of in number

595 concentration ~~on~~ of each raindrop size ~~increases~~ became significantly larger, ~~Especially especially in~~ at the interior sites ~~inside~~ mountains. The most ~~contribution~~ to the total rainfall at different sites is C2 class and C3 class next, with ~~the sum of contribution reaching 60%~~. Besides, ~~classes~~ the C5 and C6 class ~~havemade~~ a relatively large contribution to the northern slopes, with a greater probability of heavy precipitation events.

601 3. ~~There is a rather clear boundary in the distribution of $\log_{10}N_w$ versus D_m between~~ the rainfall types, which the split line between stratiform and convective rainfall ~~has the same slope with the line given by Bringi et al.~~ The dispersion degree of ~~$\log_{10}N_w$ and D_m at the six sites was~~ are 8.3% and 10.0% for stratiform rainfall and 10.4% and 23.4% for convective rainfall, respectively. ~~It is easier to increase the~~ number concentration of large raindrops in the interior area of the mountains ~~during convective rainfall~~ The standard deviations of DSD parameters ~~on inside sites are larger, making it easier to increase the number concentration of large~~ raindrops in convective rainfall. ~~Meanwhile, there is a greater increase in the~~ number concentration of raindrops over the northern slopes during convective rainfall.

612 4. ~~The Z-R relationships of different sites in stratiform rainfall are similar and~~ generally underestimated by the $Z=200R^{1.6}$ model used to the midlatitude stratiform rainfall; ~~the Z-R relationships for convective precipitation vary greatly~~ at different station, which are overestimated by $Z=300R^{1.4}$ at lower rain rates values and underestimated at higher rain rates values. The dispersion degree of coefficient A and exponent b in the Z-R relationship for the six sites ~~was~~ are 42.5% and 10.7%, respectively. Overall, ~~the Z-R relationships of the ipsilateral sites were~~ more consistent; and the A value of stratiform rainfall ~~increases~~ increased from the southern slopes to northern slopes, while the ~~opposite was true for~~ convective rainfall ~~is opposite. And the Z-R relationships of the ipsilateral sites are more~~ consistent. ~~The Z-R relationships of different sites in stratiform rainfall are~~ were similar and generally underestimated by the $Z=200R^{1.6}$ model used to the for midlatitude stratiform rainfall; ~~and the Z-R relationships for convective~~ precipitation ~~vary~~ varied greatly at different stations, which ~~are~~ were overestimated by $Z=300R^{1.4}$ at lower rain rates values and underestimated at higher rain rates values.

628 5. ~~The analysis of DSD and DSD parameters can reflect the characteristics of the~~ southern slope, northern slope and inside sites, as well as the differences between the eastern and middle sections of Qilian Mountains.

631 This study reveals the microphysical variability of precipitation ~~in~~ over the complex topography of the arid and semi-arid regions of Northwest China, which can not only improve local numerical simulations, but also provides a basis for further understanding of the differences in DSD characteristics formed at the mesoscale due to topographic factors and the water vapor distribution, etc. ~~This study~~ holds ~~is~~ importance ~~important~~ as a basis to note that this should be one of the fundamental studies for the future implementation of weather modification techniques, which is of great

带格式的: 字体: 倾斜

带格式的: 字体: 倾斜

带格式的: 字体: 倾斜

带格式的: 字体: 倾斜

带格式的: 字体: 倾斜

带格式的: 字体: 倾斜

带格式的: 字体: 倾斜

带格式的: 字体: 倾斜

带格式的: 字体: 倾斜

带格式的: 字体: 倾斜

带格式的: 字体: 倾斜

带格式的: 字体: 倾斜

638 significance ~~to~~in solving the shortage of water resources in the arid and semi-arid
639 regions.

640 *Data availability.* Disdrometer data used in this study are available by contacting the
641 authors.

642 *Author contributions.* WM conducted the detailed analysis; WZ provided financial
643 support and conceived the idea; MK collated the observation data; all the authors
644 contributed to the writing and revisions.

645 *Competing interests.* The authors declare that they have no conflict of interest.

646 **Acknowledgments**

647 The work was supported by Weather modification ability construction project of
648 Northwest China under grant No. ZQC-R18208 and The Second Tibetan Plateau
649 Comprehensive Scientific Expedition Grant No. 2019QZKK0104. Thanks are given to
650 Asi Zhang for her help in discussing some questions. The authors also thank reviewers
651 and editors for their helpful suggestion for this study

652 **References**

- 653 Adirosi, E., N. Roberto, M. Montopoli, E. Gorgucci, and L. Baldini, 2018: Influence of
654 disdrometer type on weather radar algorithms from measured DSD: Application
655 to Italian climatology. *Atmosphere*, 9, 360.
- 656 Angulo-Martínez, M., and A. Barros, 2015: Measurement uncertainty in rainfall kinetic
657 energy and intensity relationships for soil erosion studies: An evaluation using
658 PARSIVEL disdrometers in the Southern Appalachian Mountains.
659 *Geomorphology*, 228, 28-40.
- 660 Atlas, D., R. Srivastava, and R. S. Sekhon, 1973: Doppler radar characteristics of
661 precipitation at vertical incidence. *Reviews of Geophysics*, 11, 1-35.
- 662 Bringi, V., V. Chandrasekar, J. Hubbert, E. Gorgucci, W. Randeu, and M. Schoenhuber,
663 2003: Raindrop size distribution in different climatic regimes from disdrometer
664 and dual-polarized radar analysis. *Journal of the atmospheric sciences*, 60, 354-
665 365.
- 666 Campos, E., I. Zawadzki, M. Petitdidier, and W. Fernandez, 2006: Measurement of
667 raindrop size distributions in tropical rain at Costa Rica. *Journal of Hydrology*,
668 328, 98-109.
- 669 Chen, B., J. Yang, and J. Pu, 2013: Statistical characteristics of raindrop size
670 distribution in the Meiyu season observed in eastern China. *Journal of the*
671 *Meteorological Society of Japan. Ser. II*, 91, 215-227.
- 672 Dolan, B., B. Fuchs, S. Rutledge, E. Barnes, and E. Thompson, 2018: Primary modes
673 of global drop size distributions. *Journal of the Atmospheric Sciences*, 75, 1453-
674 1476.
- 675 Das, S., and A. Maitra, 2018: Characterization of tropical precipitation using drop size
676 distribution and rain rate-radar reflectivity relation. *Theoretical and applied*
677 *climatology*, 132, 275-286.
- 678 Fu, Z., and Coauthors, 2020: Statistical characteristics of raindrop size distributions and
679 parameters in Central China during the Meiyu seasons. *Journal of Geophysical*
680 *Research: Atmospheres*, 125, e2019JD031954.
- 681 Fulton, R. A., J. P. Breidenbach, D.-J. Seo, D. A. Miller, and T. O'Bannon, 1998: The
682 WSR-88D rainfall algorithm. *Weather and forecasting*, 13, 377-395.
- 683 Geoffroy, O., A. Siebesma, and F. Burnet, 2014: Characteristics of the raindrop
684 distributions in RICO shallow cumulus. *Atmospheric Chemistry and Physics*, 14,
685 10897-10909.
- 686 Ghada, W., A. Buras, M. Lüpke, C. Schunk, and A. Menzel, 2018: Rain microstructure
687 parameters vary with large-scale weather conditions in Lausanne, Switzerland.
688 *Remote Sensing*, 10, 811.
- 689 Giannetti, F., and Coauthors, 2017: Real-time rain rate evaluation via satellite downlink
690 signal attenuation measurement. *Sensors*, 17, 1864.
- 691 Gou, X., F. Chen, M. Yang, J. Li, J. Peng, and L. Jin, 2005: Climatic response of thick
692 leaf spruce (*Picea crassifolia*) tree-ring width at different elevations over Qilian
693 Mountains, northwestern China. *Journal of Arid Environments*, 61, 513-524.

- 694 [Guyot, A., Pudashine, J., Protat, A., Uijlenhoet, R., Pauwels, V., Seed, A., and Walker,](#)
695 [J. P., 2019: Effect of disdrometer type on rain drop size distribution](#)
696 [characterisation: A new dataset for south-eastern Australia. *Hydrology and Earth*](#)
697 [System Sciences, 23, 4737-4761.](#)
- 698 Jash, D., E. Resmi, C. Unnikrishnan, R. Sumesh, T. Sreekanth, N. Sukumar, and K.
699 Ramachandran, 2019: Variation in rain drop size distribution and rain integral
700 parameters during southwest monsoon over a tropical station: An inter-comparison
701 of disdrometer and Micro Rain Radar. *Atmospheric Research*, 217, 24-36.
- 702 [Jaffrain, J., and Berne, A., 2011: Experimental quantification of the sampling](#)
703 [uncertainty associated with measurements from PARSIVEL disdrometers. *Journal*](#)
704 [of Hydrometeorology, 12, 352-370.](#)
- 705 Kruger, A., and W. F. Krajewski, 2002: Two-dimensional video disdrometer: A
706 description. *Journal of Atmospheric and Oceanic Technology*, 19, 602-617.
- 707 Le Loh, J., D.-I. Lee, and C.-H. You, 2019: Inter-comparison of DSDs between
708 Jincheon and Miryang at South Korea. *Atmospheric Research*, 227, 52-65.
- 709 Li, Z., and Coauthors, 2019: Climate background, relative rate, and runoff effect of
710 multiphase water transformation in Qilian Mountains, the third pole region.
711 *Science of The Total Environment*, 663, 315-328.
- 712 Lim, Y. S., J. K. Kim, J. W. Kim, B. I. Park, and M. S. Kim, 2015: Analysis of the
713 relationship between the kinetic energy and intensity of rainfall in Daejeon, Korea.
714 *Quaternary International*, 384, 107-117.
- 715 Ma, L., L. Zhao, D. Yang, Y. Xiao, L. Zhang, and Y. Qiao, 2019a: Analysis of Raindrop
716 Size Distribution Characteristics in Permafrost Regions of the Qinghai-Tibet
717 Plateau Based on New Quality Control Scheme. *Water*, 11, 2265.
- 718 Ma, Y., G. Ni, C. V. Chandra, F. Tian, and H. Chen, 2019b: Statistical characteristics of
719 raindrop size distribution during rainy seasons in the Beijing urban area and
720 implications for radar rainfall estimation. *Hydrology and Earth System Sciences*,
721 23, 4153-4170.
- 722 Marshall, J. S., 1948: The distribution of raindrops with size. *J. meteor.*, 5, 165-166.
- 723 McFarquhar, G. M., T.-L. Hsieh, M. Freer, J. Mascio, and B. F. Jewett, 2015: The
724 characterization of ice hydrometeor gamma size distributions as volumes in N_0 -
725 λ - μ phase space: Implications for microphysical process modeling. *Journal of*
726 *Atmospheric Sciences*, 72, 892-909.
- 727 Narayana Rao, T., N. Kirankumar, B. Radhakrishna, and D. Narayana Rao, 2006: On
728 the variability of the shape-slope parameter relations of the gamma raindrop size
729 distribution model. *Geophysical research letters*, 33.
- 730 Protat, A., and Coauthors, 2019: The latitudinal variability of oceanic rainfall properties
731 and its implication for satellite retrievals: 1. Drop size distribution properties.
732 *Journal of Geophysical Research: Atmospheres*, 124, 13291-13311.
- 733 Pu, K., X. Liu, Y. Wu, S. Hu, L. Liu, and T. Gao, 2020: A comparison study
734 of raindrop size distribution among five sites at the urban scale during the
735 East Asian rainy season. *Journal of Hydrology*, 590, 125500, <https://doi.org/>

736 [g/10.1016/j.jhydrol.2020.125500](https://doi.org/10.1016/j.jhydrol.2020.125500).

737 Penide, G., A. Protat, V. V. Kumar, and P. T. May, 2013: Comparison of two
738 convective/stratiform precipitation classification techniques: Radar reflectivity
739 texture versus drop size distribution–based approach. *Journal of Atmospheric and*
740 *Oceanic Technology*, 30, 2788-2797.

741 Qin, Y., H. Lei, D. Yang, B. Gao, Y. Wang, Z. Cong, and W. Fan, 2016: Long-term
742 change in the depth of seasonally frozen ground and its ecohydrological impacts
743 in the Qilian Mountains, northeastern Tibetan Plateau. *Journal of Hydrology*, 542,
744 204-221.

745 Rincon, R. F., and R. H. Lang, 2002: Microwave link dual-wavelength measurements
746 of path-average attenuation for the estimation of drop size distributions and rainfall.
747 *IEEE Transactions on geoscience and remote sensing*, 40, 760-770.

748 Raupach, T. H., M. Thurai, V. Bringi, and A. Berne, 2019: Reconstructing the drizzle
749 mode of the raindrop size distribution using double-moment normalization.
750 *Journal of Applied Meteorology and Climatology*, 58, 145-164.

751 Seela, B. K., J. Janapati, P. L. Lin, K. K. Reddy, R. Shirooka, and P. K. Wang, 2017: A
752 comparison study of summer season raindrop size distribution between Palau and
753 Taiwan, two islands in western Pacific. *Journal of Geophysical Research: Atmospheres*, 122, 11,787-711,805.

755 Smith, J. A., E. Hui, M. Steiner, M. L. Baeck, W. F. Krajewski, and A. A. Ntelekos,
756 2009: Variability of rainfall rate and raindrop size distributions in heavy rain.
757 *Water Resources Research*, 45.

758 Thurai, M., P. Gatlin, and V. Bringi, 2016: Separating stratiform and convective rain
759 types based on the drop size distribution characteristics using 2D video
760 disdrometer data. *Atmospheric Research*, 169, 416-423.

761 Thurai, M., P. Gatlin, V. Bringi, W. Petersen, P. Kennedy, B. Notaroš, and L. Carey,
762 2017: Toward completing the raindrop size spectrum: Case studies involving 2D-
763 video disdrometer, droplet spectrometer, and polarimetric radar measurements.
764 *Journal of Applied Meteorology and Climatology*, 56, 877-896.

765 Testud, J., S. Oury, R. A. Black, P. Amayenc, and X. Dou, 2001: The concept of
766 “normalized” distribution to describe raindrop spectra: A tool for cloud physics
767 and cloud remote sensing. *Journal of Applied Meteorology*, 40, 1118-1140.

768 Tian, H., T. Yang, and Q. Liu, 2014: Climate change and glacier area shrinkage in the
769 Qilian mountains, China, from 1956 to 2010. *Annals of Glaciology*, 55, 187-197.

770 [Ulbrich C W., 1983: Natural variations in the analytical form of the raindrop size](#)
771 [distribution. *Journal of climate and applied meteorology*, 22, 1764-1775.](#)

772 Wainwright, C. E., D. T. Dawson, M. Xue, and G. Zhang, 2014: Diagnosing the
773 intercept parameters of the exponential drop size distributions in a single-moment
774 microphysics scheme and impact on supercell storm simulations. *Journal of*
775 *Applied Meteorology and Climatology*, 53, 2072-2090.

776 Wang, Y., J. Zheng, Z. Cheng, and B. Wang, 2020: Characteristics of Raindrop Size
777 Distribution on the Eastern Slope of the Tibetan Plateau in Summer. *Atmosphere*,

778 11, 562.
779 Wu, Y., and L. Liu, 2017: Statistical characteristics of raindrop size distribution in the
780 Tibetan Plateau and southern China. *Advances in Atmospheric Sciences*, 34, 727-
781 736.
782 Yang, L., J. Smith, M. L. Baeck, B. Smith, F. Tian, and D. Niyogi, 2016: Structure and
783 evolution of flash flood producing storms in a small urban watershed. *Journal of*
784 *Geophysical Research: Atmospheres*, 121, 3139-3152.
785 Zhang, A., and Coauthors, 2019: Statistical characteristics of raindrop size distribution
786 in the monsoon season observed in southern China. *Remote Sensing*, 11, 432.
787 Zhao, P., and Coauthors, 2019: The Tibetan Plateau surface-atmosphere coupling
788 system and its weather and climate effects: The Third Tibetan Plateau Atmospheric
789 Science Experiment. *Journal of Meteorological Research*, 33, 375-399.
790 Zeng, Y., and Coauthors, 2021: Statistical Characteristics of Raindrop Size Distribution
791 during Rainy Seasons in Northwest China. *Advances in Meteorology*, 2021.
792